Antonio Soria-Verdugo, Mariano Rubio-Rubio, Elke Goos, Uwe Riedel,

On the characteristic heating and pyrolysis time of thermally small biomass particles in a bubbling fluidized bed reactor,

Renewable Energy 160 (2020) 312-322.

The original publication is available at www.elsevier.com
https://doi.org/10.1016/j.renene.2020.07.008

On the characteristic heating and pyrolysis time of thermally small biomass particles in a bubbling fluidized bed reactor

Antonio Soria-Verdugo[a]*, Mariano Rubio-Rubio[a], Elke Goos[b], Uwe Riedel[b]

[a] *Carlos III University of Madrid (Spain), Department of Thermal and Fluids Engineering. Avda. de la Universidad 30, 28911 Leganés (Madrid, Spain).*

[b] *Deutsches Zentrum für Luft- und Raumfahrt e.V. (German Aerospace Center, DLR), Institute of Combustion Technology, Pfaffenwaldring 38-40, 70569 Stuttgart (Germany).*

** corresponding author: asoria@ing.uc3m.es Tel: +34916248465.*

Abstract

Pyrolysis of crushed olive stone particles in a lab scale Bubbling Fluidized Bed (BFB) reactor was investigated. The time evolution of the pyrolysis conversion degree of the olive stone particles, while moving freely in the BFB, was determined from the evolution of the mass of olive stones remaining in the bed, measured by a precision scale holding the whole reactor installation. The experimental measurements of the pyrolysis conversion degree were employed to validate a simple model combining heat transfer and chemical kinetics, which is valid for thermally small particles. The model combines the Lumped Capacitance Method (LCM) and the simplified Distributed Activation Energy Model (DAEM) to account for heat transfer and pyrolysis chemical kinetics, respectively. The estimations of the combined LCM-DAEM model for the pyrolysis conversion degree were found to be in good agreement with the

experimental measurements for the pyrolysis of olive kernels in a BFB operated at various bed temperatures, fluidizing gas velocities, and biomass particle size ranges. From the combined LCM-DAEM model, the characteristic heating time and the pyrolysis time of the olive stone particles were derived, obtaining a direct relation between these two parameters for constant values of the bed temperature.

Keywords**:** Olive stones pyrolysis; Bubbling fluidized bed (BFB); Characteristic heating time; Characteristic pyrolysis time; Distributed Activation Energy Model (DAEM); Lumped Capacitance Method (LCM).

Nomenclature

A	Pre-exponential factor [s^{-1}]
A_s	Surface of the solid particle [m^2]
α	Pyrolysis conversion degree [%]
Bi	Biot number [-]
β	Heating rate [ºC min^{-1}]
c	Heating parameter [s^{-1}]
c_s	Specific heat of the solid particle [J kg^{-1} K^{-1}]
d_{os}	Particle size of olive stones [mm]
E	Activation energy [kJ mol^{-1}]
ϕ_{ie}	Value of the ϕ-function for which the step function changes [-]
h	Convection coefficient [W m^{-2} K^{-1}]
k_s	Thermal conductivity of the solid particle [W m^{-1} K^{-1}]
L_c	Characteristic length [m]
m	Mass of olive stones remaining in the bed [kg]

m_0 Initial mass of olive stones supplied to the bed [kg]

m_{sr} Mass of solid residue remaining after the pyrolysis process [kg]

ρ_s Density of the solid particle [kg m^{-3}]

R Universal gas constant [J mol^{-1} K^{-1}]

t Time [s]

t_{pyr} Characteristic pyrolysis time [s]

T Temperature [ºC]

T_0 Ambient temperature [ºC]

T_∞ Reactor temperature [ºC]

τ Characteristic heating time [s]

U Inert gas velocity [m/s]

U_{mf} Minimum fluidization velocity of the bed material [m/s]

U/U_{mf} Dimensionless gas velocity [-]

V_s Volume of the solid particle [m^3]

X Percentage of mass of olive stones remaining in the bed [%]

Abbreviations:

DAEM Distributed Activation Energy Model

DTG Differential Thermogravimetric

HHV High Heating Value

LCM Lumped Capacitance Method

OS Olive Stones

TG Thermogravimetric

TGA Thermogravimetric Analyzer

1. Introduction

Pyrolysis is a promising technology to obtain a high-quality liquid bio-fuel from the thermal degradation of solid biomass particles. During pyrolysis, the thermal degradation of biomass occurs in absence of oxygen, producing a solid residue (bio-char) and pyrolysis vapors, which can be subjected to a condensation process to obtain a liquid fuel (bio-fuel) and a flow of permanent gases. Compared to other thermochemical processes employed to convert biomass, pyrolysis has some advantages, e.g., using moderate temperatures ranging from 300 to 600 °C, obtaining high-quality products from the conversion, and producing a reduced amount of pollutant emission resulting from the conversion, compared to other technologies.

The quantity and quality of the solid, liquid and gaseous yields obtained from pyrolysis depends strongly on the characteristics of the biomass and the operating conditions employed during the process [1]. The main operating conditions affecting the generation of bio-oil from biomass pyrolysis are the reactor temperature, the heating rate of the biomass particles, the residence time of the pyrolysis vapors, and the biomass particle size. A maximum production of bio-oil is obtained for intermediate temperatures, thus avoiding secondary cracking reactions occurring for temperatures above 600 ºC, which enhance the production of permanent gases [2]. Fast heating rates, short residence time of the pyrolysis vapors and small biomass particle sizes are also recommended to maximize the generation of bio-oil by limiting these secondary cracking reactions [3]. These are the characteristics of the so-called fast pyrolysis processes, used to convert solid biomass into high-quality bio-oil [4].

However, the range of variability of these operating conditions and the capability to control them are specific characteristics of the pyrolysis reactor employed.

Numerous reactor designs and technologies are applied to hold biomass pyrolysis reactions, including fixed beds [5], fluidized beds [6], spouted beds [7], rotating cone reactors [8], ablative reactors [9], rotary kiln reactors [10], auger reactors [11], drop tube reactors [12], microwave reactors [13], vacuum reactors [14], plasma reactors [15], and Curie-point reactors [16]. Among the different reactors available, bubbling fluidized beds inherently have the appropriate characteristics to hold fast pyrolysis reactions of biomass, enabling a stable and homogeneous temperature operation and providing high heating rates to the biomass particles while limiting the residence time of the pyrolysis vapors in the hot zone of the reactor. Several kinetic models are available in the literature to describe biomass pyrolysis kinetics, such as single step models [17], three pseudo-components models [18], isoconversional models [19], or the Distributed Activation Energy Model (DAEM) [20]. However, no heat and mass transfer effects inside the biomass are considered in these kinetic models, although the kinetic models can be combined with heat transfer models to take into account these effects [21]. Furthermore, these kinetic models are typically validated with experimental measurements conducted under the controlled conditions of a thermogravimetric analyzer, where other factors of the reactor geometry, e.g., fluid-dynamics, are ignored. In this regard, a macro-TGA, consisting of a lab-scale bubbling fluidized bed reactor installed over a precision scale, capable of detecting the mass released by biomass particles during their pyrolysis, can provide valuable measurements to validate pyrolysis models,

considering both kinetics and heat transfer effects during biomass pyrolysis, together with fluid-dynamics effects of the reactor [22,23].

In this work, a simple model combining heat transfer and chemical kinetics is applied to describe the evolution of the pyrolysis process of crushed olive stones in a bubbling fluidized bed. This work presents two main novelties: the use of an original non-intrusive measuring technique to determine the time evolution of the conversion degree during pyrolysis of biomass in a BFB reactor and the proposal of a simple model to describe the pyrolysis process, considering both heat transfer and chemical kinetics. The model uses the simplified Distributed Activation Energy Model (DAEM) to account for the chemical kinetics of pyrolysis and the Lumped Capacitance Method (LCM) to describe the transient heat transfer in the biomass particles. Thus, the combined LCM-DAEM model is only valid for thermally small particles, for which LCM is applicable. The combined model was validated by comparing the time evolution of the mass of small olive stone particles during their pyrolysis in a bubbling fluidized bed measured by a scale to the estimation of the model, obtaining both the heating and the pyrolysis time of the samples as a function of the operating conditions, i.e., bed temperature, inert gas velocity, and olive stone particle size.

2. Pyrolysis model for thermally small particles

The pyrolysis of solid biomass particles is a complex process involving both chemical kinetics and heat and mass transfer. In this work, the pyrolysis of thermally small olive stone particles is modelled by a combined heat transfer and chemical kinetics model. In the combined model, the simplified Distributed

Activation Energy Model (DAEM) accounts for the pyrolysis chemical kinetics, whereas the transient heat transfer to the biomass particles is described by the Lumped Capacitance Method (LCM).

2.1. Lumped Capacitance Method (LCM)

The Lumped Capacitance Method (LCM) is widely used to describe transient conduction problems in which the thermal resistance by conduction inside the solid particle is negligible compared to the thermal resistance by convection at its surface, i.e., the Biot number is negligibly low, $Bi = h \cdot L_c / k_s$, where h is the convective coefficient, k_s is the thermal conductivity of the biomass particle, and L_c is the characteristic length determined as the volume to surface ratio of the particle, $L_c = V_s/A_s$. Under this assumption, the temperature T inside the particle can be considered spatially uniform, that is, independent of the particle radius, and thus the particle temperature is an exclusive function of time during the heating process. In practical applications, the LCM can be applied with a limited error for $Bi \leq 0.1$ [24], which is the condition under which the particles are called *thermally small particles*.

Considering a solid particle with a volume V_s and an external surface A_s, a particle density ρ_s, and a specific heat c_s, with an initial temperature T_0, entering in a reactor at a constant temperature T_∞, the time evolution of a thermally small solid particle described by the LCM is an inverse exponential approximation to the reactor temperature, in the form

$$\frac{T_\infty - T}{T_\infty - T_0} = \exp\left(-\frac{h \cdot A_s}{\rho_s \cdot V_s \cdot c_s} t \right). \quad (1)$$

The coefficient multiplying time in Eq. (1) is the heating parameter *c*, whose reciprocal value is the characteristic heating time τ of the solid particle, defined as follows:

$$\tau = \frac{\rho_s \cdot V_s \cdot c_s}{h \cdot A_s}. \tag{2}$$

2.2. Simplified Distributed Activation Energy Model (DAEM)

The Distributed Activation Energy Model considers the pyrolysis of a solid fuel to be composed of a large number of first order reactions, occurring simultaneous or consecutively, which are assumed to be independent from each other. Additionally, all reverse reactions and their dependence from thermodynamic properties are ignored. According to DAEM, the conversion degree α during pyrolysis of a solid fuel can be determined as follows:

$$1-\alpha = \int_0^\infty \exp\left(-A\int_0^t \mathrm{e}^{E/RT}\,\mathrm{d}t\right) f\left(E\right)\cdot \mathrm{d}E, \tag{3}$$

where α is the pyrolysis conversion at time *t*, *A* is the pre-exponential factor, *E* is the activation energy, *R* is the universal gas constant, *T* is the temperature, and *f(E)* is the probability density function of the activation energy.

DAEM was simplified by Miura [25] and Miura and Maki [26], considering the exponential term in Eq. (3), the so-called ϕ function, as a step function. Using this simplification and the approximation of Coats and Redfern [17] for the temperature integral, Miura and Maki [26] derived the Arrhenius equation for the simplified DAEM

$$\ln\left(\frac{\beta}{T^2}\right)=\ln\left(\frac{AR}{E}\right)+0.6075-\frac{E}{R}\frac{1}{T}, \quad (4)$$

which relates the temperature T at which each conversion degree α occurs with the pre-exponential factor A, activation energy E, gas universal constant R, and heating rate β. This Arrhenius equation of simplified DAEM has been used by several authors to derive the kinetic parameters, A and E, of a broad variety of solid fuels [27-36]. However, the validity of this equation is restricted only to constant heating rates, i.e., linear increase of temperature. In this regard, Soria-Verdugo et al. [37] derived similar Arrhenius equations valid for the pyrolysis of solid fuels under parabolic and positive exponential temperature increases. Also, Soria-Verdugo et al. [21] proposed an Arrhenius equation valid for inverse exponential temperature increases, combining the LCM and simplified DAEM to describe the pyrolysis of thermally small solid particles.

2.3. Combined LCM and simplified DAEM (LCM-DAEM)

In a previous work, Soria-Verdugo et al. [21] followed a similar mathematical procedure to that proposed by Miura [25] to derive an Arrhenius equation, based on simplified DAEM, valid for inverse exponential temperature profiles as those predicted by the LCM for thermally small particles, yielding:

$$\ln\left(\frac{T_\infty-T}{\tau\cdot T^2}\right)=\ln\left(\frac{AR}{E}\right)-\ln\left(-\ln\left(\phi_{ie}\right)\right)-\frac{E}{R}\frac{1}{T}. \quad (5)$$

The value of ϕ_{ie} in Eq. (5) is a parabolic function of the reactor temperature T_∞ in the form ϕ_{ie} = -1.533·10^{-6}· T_∞^2 + 2.577·10^{-3}· T_∞ – 0.4745, with T_∞ in ºC. Since Eq. (5) is valid for the whole conversion range, it could be solved to determine the temperature for which each conversion degree occurs. It can be derived as

long as the evolution of the kinetic parameters E and A with the conversion degree, the reactor temperature T_∞, and the characteristics of the biomass particles required to determine τ are known. The validity of Eq. (5) to describe the pyrolysis of various biomass types under inverse exponential temperature increases was proved by Soria-Verdugo et al. [21], for pyrolysis measurements conducted in a thermogravimetric analyzer. However, since this validation was based on TGA measurements, no fluid-dynamics effects on the pyrolysis imposed by the reactor were considered. In this work, the combined LCM-DAEM model described by Eq. (5) will be employed to describe the pyrolysis of crushed olive stones in a more complex reactor, a bubbling fluidized bed, where the bed fluid-dynamics will play an important role on the pyrolysis process.

3. Materials and Methods

3.1. Biomass Characterization

Olive stones are a residue from the olive oil industry, generated in large quantities in southern Europe, whose energy content can be utilized in several ways [38]. The crushed olive stones investigated in this paper were bought from the company Olihueso (Cordoba, Spain) in January 2019. They were milled to a particle size below 100 μm before their basic characterization. The basic characterization carried out includes proximate and ultimate analyses, carried out respectively in a TGA Q500 from TA Instruments and in a LECO TruSpec CHN Macro and TruSpec S analyzer. A heating value test of the biomass samples was also performed in a Parr 6300 isoperibolic calorimeter. The results obtained from the basic characterization of the olive stone particles are reported in Table 1, reported as an average value of three repetitions in each case. Olive

stones are characterized by high volatile matter and carbon contents. In contrast, the contents of ash, nitrogen and sulfur are reduced, limiting emission of pollutants such as nitro oxides and sulfur oxides and reducing corrosion problems derived from ash melting [39]. Further details of the basic characterization can be found in Soria-Verdugo et al. [40].

Table 1. Results of the basic characterization of olive stones (PA: Proximate Analysis, UA: Ultimate Analysis, VM: Volatile Matter, FC: Fixed Carbon, A: Ash, C: Carbon, H: Hydrogen, N: Nitrogen, S: Sulfur, O: Oxygen, HHV: High Heating Value, db: dry basis, daf: dried ash free basis, * calculated by difference).

PA [%db]			UA [%daf]					HHV
VM	FC*	A	C	H	N	S	O*	[MJ/kg db]
77.0	22.3	0.7	52.4	6.1	0.9	0.1	40.5	20.1

3.2. Experimental facility and procedure

The experimental setup consists of a lab scale bubbling fluidized bed (BFB) reactor, with an inner diameter of 4.7 cm, installed on a precision scale model PS 6000 R2 from RADWAG. The wall of the reactor was surrounded by three electric resistors that supply the thermal power required to heat up the bed to the desired temperature. Glass wool was used as insulator to minimize heat losses through the reactor wall. The reactor was made of stainless steel. The mass of the whole reactor, including the vessel, electric resistors and thermal insulation, was selected to be 5.5 kg, since the maximum mass measurable by the scale is 6 kg. The 5.5 kg of the whole reactor were adjusted by including a mass of around 2 kg at the bottom of the reactor to improve its stability during the measurements.

Nitrogen was used as fluidizing agent. The flow rate of nitrogen was measured by a flowmeter PFM710-C6-E from SMC and it was supplied to the plenum chamber through a flexible pipe to avoid any interference with the mass measurement of the scale. The exhaust nitrogen fluidizing the bed and the pyrolysis vapors released during the biomass conversion were collected by a suction pipe located around 0.5 m above the top of the reactor and circulated to the chimney. The suction pipe was not in direct contact to the top of the reactor to avoid any disturbance of the scale measurement and the suction rate of the pipe was limited to ensure no suction effect on the pyrolysis reactor. Therefore, during the measurement of the mass released by the biomass samples pyrolyzing in the bubbling fluidized bed, the only connection to the reactor was the flexible pipe supplying the fluidizing nitrogen, which was proved to have no effect of the scale measurement.

Silica sand with an average particle size of 275 μm was employed as bed material due to its inert character during biomass thermochemical conversion [41]. For each test, a mass of 227 g of fresh silica sand particles was used, corresponding to a static bed height of 9.4 cm. Further details of the experimental facility can be found in Soria-Verdugo et al. [22].

During the pyrolysis tests, a mass of 10 g of olive stones was supplied to the bed as a batch through the top of the reactor once the desired bed temperature was attained. The evolution of the mass was registered by the scale, initially tared before supplying the olive stones to the bed. Different tests varying bed temperatures, gas velocities, and particle sizes of the olive stones were performed during the experimental campaign. Bed temperatures T_∞ close to the optimal temperature to maximize the liquid yield obtained from pyrolysis were

tested, specifically 500, 550 and 600 ºC [42]. For these bed temperatures, the minimum fluidization velocity U_{mf} of the silica sand particles used as bed material is around 3.7 cm/s in all cases. The gas velocity was varied in a narrow range to guarantee both a proper fluidization of the bed and the operation of the bed in the bubbling fluidized bed regime. Taking into account these considerations, the dimensionless gas velocities U/U_{mf} tested were 2.5, 3.0, and 3.5, since the size of the bubbles produced at U/U_{mf} > 4.0 is comparable to the reactor diameter, resulting in an operation of the bed under the slugging regime, which is out of the scope of this work. Finally, the particle size of the olive stones pyrolyzed d_{os} was also varied, limiting the maximum value to fulfill the thermally small particle criterium. The particle sizes used during the tests were in the ranges 1.25 – 1.60, 1.60 – 2.00, 2.00 – 2.50, and 2.50 – 3.15 mm. Each test was replicated to check the repeatability of the experimental measurement obtaining deviations below 3% between replicates in all cases. A total of 16 pyrolysis tests, considering the replicates, were conducted varying the operating parameters as indicated in Table 2.

Table 2. Pyrolysis experiments conducted in the BFB reactor.

Experiment	T_∞ **[ºC]**	U/U_{mf} **[-]**	d_{os} **[mm]**
1	500	3.0	1.25 – 1.60
2	500	2.5	1.25 – 1.60
3	500	3.5	1.25 – 1.60
4	550	3.0	1.25 – 1.60
5	600	3.0	1.25 – 1.60
6	550	3.0	1.60 – 2.00
7	550	3.0	2.00 – 2.50
8	550	3.0	2.50 – 3.15

No dragging of biomass or bed material was detected during the experimental campaign for any of the operating conditions tested, specified in Table 2. In fact, dragging was first detected for much higher dimensionless gas velocity, almost double, compared to those considered in this study.

4. Results and Discussion

4.1. Pyrolysis kinetics of olive stones

Simplified DAEM was first applied to determine the kinetic parameters of the olive stone during its pyrolysis, i.e., the pre-exponential factor *A* and the activation energy *E*. To obtain accurate values for *A* and *E*, nine pyrolysis experiments were conducted in the TGA Q500 using constant heating rates of β = 10, 13, 16, 19, 22, 25, 30, 35 and 40 K/min, following the procedure described by Soria-Verdugo et al. [40]. Figure 1 a) shows the TG curves obtained for the olive stone pyrolysis at the nine constant heating rates tested, representing the evolution of the conversion degree α with temperature *T*. Most of the pyrolysis occurs in a narrow temperature range between 225 and 375 ºC, at higher temperatures the pyrolysis process is slow. As a result of the non-isothermal process, the pyrolysis of olive stones occurs at slightly higher temperatures when the heating rate is increased. However, the effect of the heating rate on the pyrolysis process can be observed more clearly in the DTG curves, where the conversion rate $\mathrm{d}\alpha/\mathrm{d}t$ is plotted as a function of temperature *T*. The DTG curves of olive stone pyrolysis are depicted in Figure 1 b), where an increase of the conversion rate for higher values of the heating rate is noticed. The DTG curves shown in Figure 1 b) are composed of two overlapping peaks and a third underlying peak, corresponding to the conversion of the main three pseudo-

components constituent of lignocellulosic biomass, namely hemicellulose, cellulose, and lignin. This is a typical result for pyrolysis of lignocellulosic biomass [43].

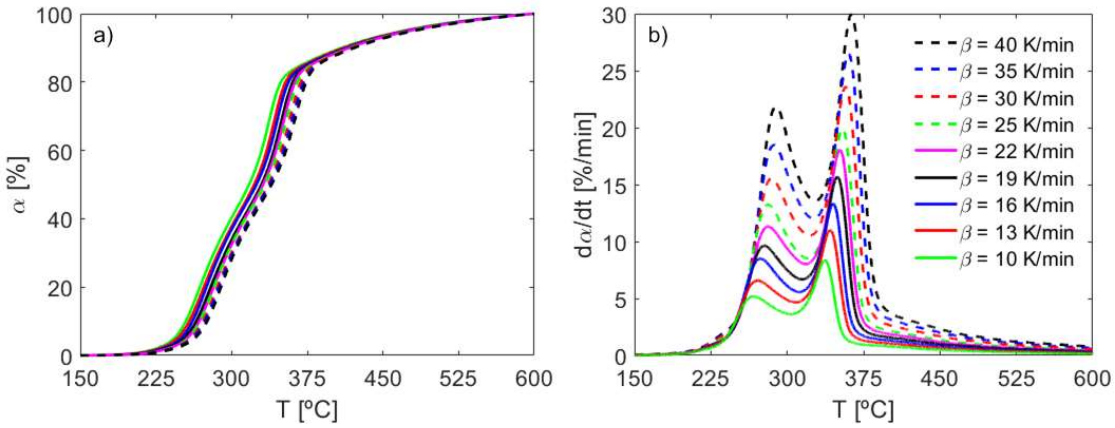

Figure 1: a) TG curves and b) DTG curves corresponding to olive stone pyrolysis in TGA at various heating rates.

The evolution of the conversion degree α with temperature T shown in the TG curves for each heating rate β can be used to build the Arrhenius plot, characteristic of the simplified DAEM. In this Arrhenius plot, $\ln(\beta/T^2)$ is represented as a function of $1/T$ for specific values of the conversion degree. Even though all calculations within this paper were carried out using intervals of 1 % for the pyrolysis conversion, α, in a range from 5 to 95 %, Figure 2 shows the Arrhenius plot, built using conversion rate intervals of 5 % to improve data visualization. A high linearity of the data obtained for the same value of the conversion degree at different heating rates can be observed visually in Figure 2. In fact, the average value of determination coefficient R^2 of the linear fitting of the data included in the Arrhenius plot is 0.989, which proves the reliability of the experimental data obtained from the pyrolysis tests conducted in the TGA [44].

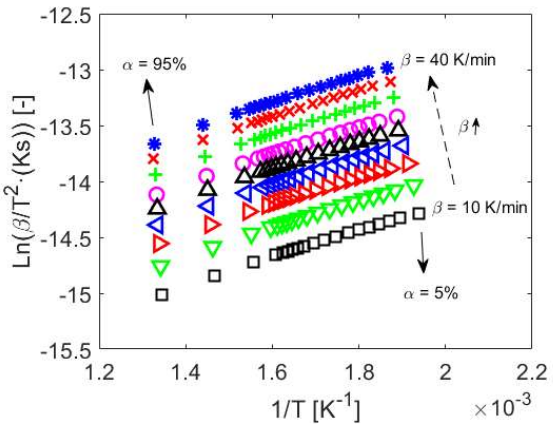

Figure 2: Arrhenius plot of the olive stone pyrolysis (intervals of 5 % were used for α to improve visualization).

Considering the Arrhenius equation for the simplified DAEM, Eq. (4), the evolution of the activation energy *E* and pre-exponential factor *A* with the conversion degree α can be obtained from the slope and intercept of the linear fitting of the data represented in the Arrhenius plot. The results obtained for the kinetic parameters of olive stone pyrolysis are represented in Figure 3, where a similar tendency is observed for both the pre-exponential factor and activation energy. In both cases, the value of the kinetic parameter is quite uniform up to a conversion degree around α = 80 %, increasing sharply at the end of the pyrolysis process, when the pyrolysis is slower as shown in Figure 3 a). The uniform value of the pre-exponential factor for conversion degrees below 80 % is around 10^{12} s^{-1}, while the activation energy is approximately 175 kJ/mol. Considering the whole pyrolysis process, the pre-exponential factor of olive stone ranges from 10^{12} to 10^{28} s^{-1} and the activation energy varies from 150 to 400 kJ/mol. The evolution of *A* and *E* with *α* will be used as an input for the LCM-DAEM model proposed to obtain the time evolution of the conversion

degree during pyrolysis of crushed olive stones in a bubbling fluidized bed, by solving Eq. (5) for specific values of α.

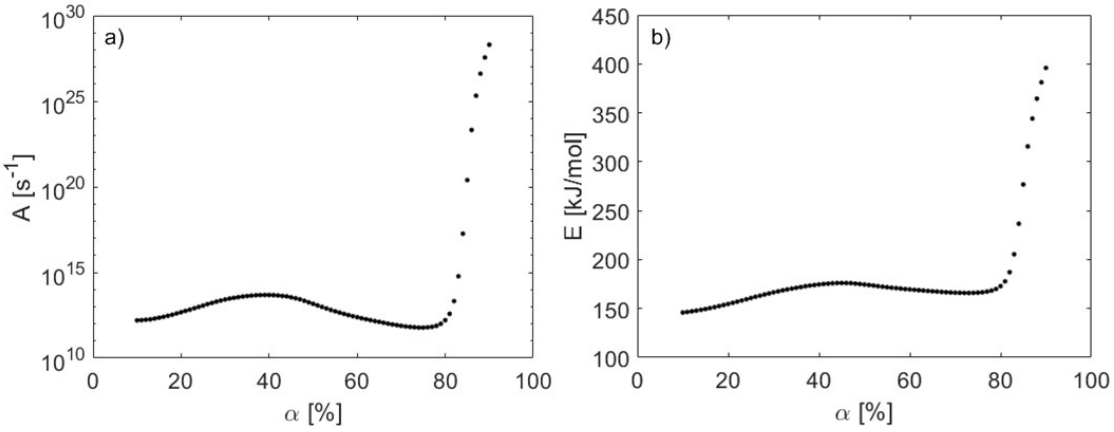

Figure 3: Kinetic parameters of the olive stone pyrolysis for a conversion degree range from 10 to 90 % in intervals of 1 %: a) pre-exponential factor *A*, b) activation energy *E*.

4.1. Pyrolysis of olive stones in a bubbling fluidized bed

The pyrolysis of olive stones as a fuel in the lab scale BFB reactor was analyzed for various values of the bed temperature T_∞, dimensionless gas velocity U/U_{mf}, and biomass particle size d_{os}, based on the time evolution of the fuel mass remaining in the reactor monitored by the scale. The original signal of the fuel mass registered by the scale can be observed in Figure 4, corresponding to the pyrolysis of olive stone particles with d_{os} = 1.15 – 1.60 mm in a BFB at T_∞ = 500 ºC operated with a dimensionless gas velocity of U/U_{mf} = 3.0. At the beginning of the test, the scale was tared, registering an average null mass of fuel. The remaining scatter is caused by the bubbling fluidized bed. After the supply of the biomass as a batch through the top of the bed, the mass suddenly increases to 10 g and the pyrolysis process starts. First, the scale measurement is quite stable during the heating of the olive stone particles.

Then, the mass of biomass inside the bed decreases as a result of the volatile matter release during pyrolysis. Finally, at the end of the test, the mass of biomass remaining in the bed is uniform, corresponding to the char generated as a solid residue of the pyrolysis process. Figure 4 shows some scattering in the mass measurement, which is due to the ascension and eruption of bubbles at the bed surface. However, this scattering is reduced, and the essential information of the olive stones mass variation during their pyrolysis can be extracted from the signal. Furthermore, using this non-intrusive measuring technique, no interference on the motion of the biomass particles is caused and the essential information of the evolution of the pyrolysis process inside the bed can be collected.

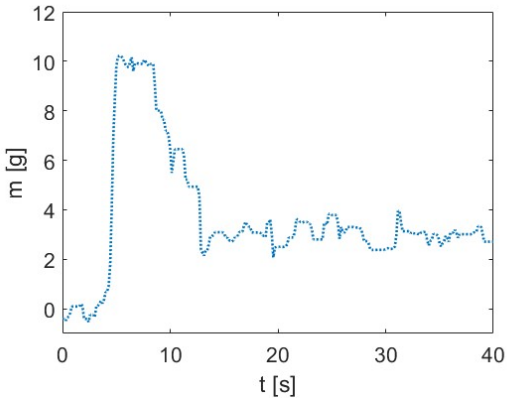

Figure 4: Time evolution of the fuel mass remaining in the bed registered by the scale (T_∞ = 500 ºC, U/U_{mf} = 3.0, d_{os} = 1.15 – 1.60 mm).

Considering the initial mass of olive stones supplied, m_0 = 10 g in all cases, the percentage of mass remaining in the reactor X can be determined as $X = m/m_0$. The time evolution of X for the pyrolysis of olive stones of d_{os} = 1.15 – 1.60 mm in a bed operated at T_∞ = 500 ºC and U/U_{mf} = 3.0 is depicted in Figure 5 a). In this figure, the initial point corresponds to the moment when the mass

measured by the scale equals the initial mass of olive stones supplied, obtaining a percentage of mass of X = 100 %, whereas at the end of the pyrolysis the percentage of mass remaining corresponds to the percentage of char generated. To remove variations caused by different char amounts produced when varying the operating conditions, the pyrolysis conversion degree α can be calculated taking into account both the initial mass of biomass supplied m_0 and the uniform mass of char generated as a solid residue m_{sr}, as follows:

$$\alpha = \frac{m_0 - m}{m_0 - m_{sr}}. \tag{6}$$

The time evolution of the pyrolysis conversion degree is represented in Figure 5 b) for the pyrolysis of olive stones of d_{os} = 1.15 – 1.60 mm in a BFB operated at T_∞ = 500 ºC and U/U_{mf} = 3.0. The pyrolysis conversion degree increases from α = 0 %, at the beginning of the pyrolysis process, to α = 100 %, when the olive stone particles are completely pyrolyzed.

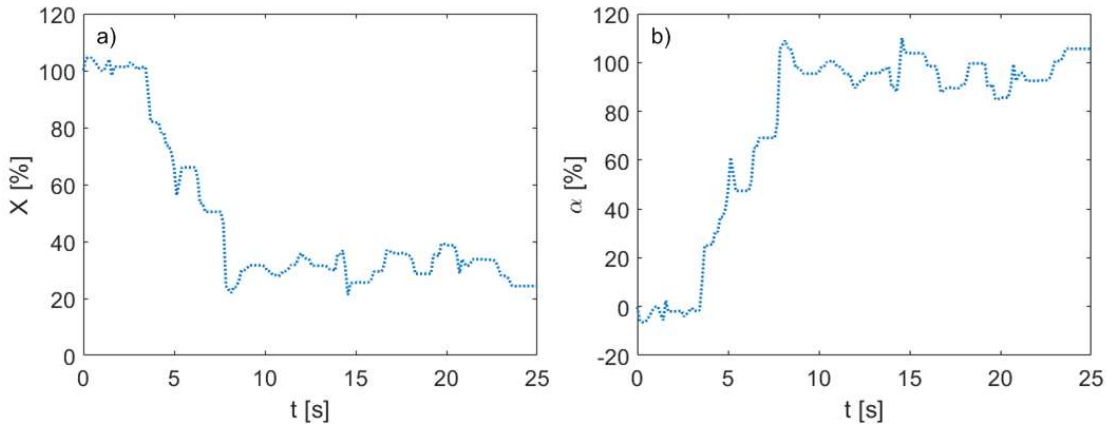

Figure 5: Time evolution of the percentage of mass remaining (a) and conversion degree (b) during the pyrolysis of olive stones in a BFB reactor (T_∞ = 500 ºC, U/U_{mf} = 3.0, d_{os} = 1.15 – 1.60 mm).

4.2. Modeling the pyrolysis of olive stones in a bubbling fluidized bed

The transcendental equation of the combined LCM-DAEM model, Eq. (5), can be solved for each value of the conversion degree α, considering the dependence of the kinetic parameters, *A* and *E*, of the olive stone pyrolysis on α, presented in Figure 3 as input data. The values used for the kinetic parameters in the combined LCM-DAEM model proposed were obtained from TGA measurements, conducted for lower heating rates compared to those expected for bubbling fluidized beds. In this work, the value of the characteristic heating time τ in Eq. (5) is obtained as free parameter of the best fitting of the combined LCM-DAEM model results to the experimental measurement of the conversion degree time evolution. However, if a proper estimation of the parameters on which τ depends were available, the value of the characteristic time could be calculated by Eq. (2) and introduced in the model as an input. Therefore, in this case, the numerical work consisted in solving Eq (5) numerically for the whole conversion degree range, from 0 to 100 %, for specific values of τ, obtaining the temperature *T* for which each value of α occurs. Considering Eq. (1), the dependence of the conversion degree α on temperature *T* can be expressed as a time dependence, taking into account the reactor temperature T_∞ and the characteristic heating time τ. Finally, the curves of α as a function of *t*, obtained for several values of τ, are compared to the experimental α-*t* curve to determine the characteristic heating time of the olive stone particles in the BFB reactor.

The comparison of the model estimation for the time evolution of the conversion degree with the experimental measurement can be observed in Figure 6, for the

pyrolysis of olive stones of d_{os} = 1.15 – 1.60 mm in a BFB at T_∞ = 500 ºC and U/U_{mf} = 3.0. Under these operating conditions, the characteristic heating time of these olive stone particles is τ = 4.0 s. Figure 6 shows the capability of the proposed LCM-DAEM model to estimate the evolution of the olive stones mass in such a complex reactor as a BFB. The model follows the tendency of the experimental measurement of the conversion degree, without any scattering due to bubbles' motion.

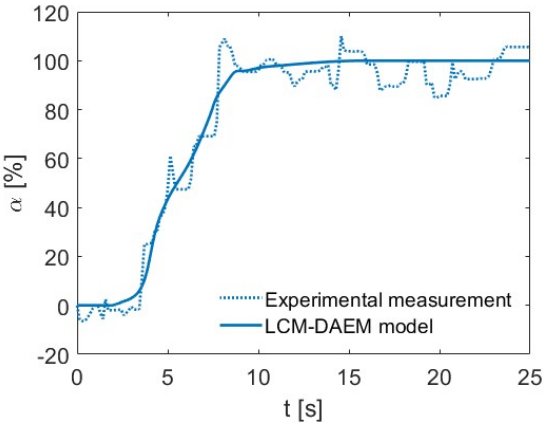

Figure 6: Comparison of the LCM-DAEM estimation and the experimental measurement for the time evolution of the conversion degree during pyrolysis of olive stones in a BFB reactor (T_∞ = 500 ºC, U/U_{mf} = 3.0, d_{os} = 1.15 – 1.60 mm).

In the following subsections, the effect of varying the different operating conditions, i.e., U/U_{mf}, T_∞, and d_{os}, is analyzed, obtaining the effect of these parameters on the characteristic heating time and the pyrolysis time, and confirming the capability of the proposed LCM-DAEM model to describe the pyrolysis of biomass in a BFB reactor.

4.3. Effect of gas velocity

The effect of the gas velocity was quantified by analyzing the pyrolysis of olive stones with particle size of d_{os} = 1.15 – 1.60 mm in a bed at T_∞ = 500 ºC, for three values of the dimensionless gas velocity of U/U_{mf} = 2.5, 3.0, and 3.5. The results of the experimental measurements of the time evolution of α are shown in Figure 7, together with the estimations of the LCM-DAEM obtained for the corresponding value of τ in each case. Increasing the gas velocity accelerates the pyrolysis process, displacing the conversion degree curves to shorter times, due to an enhancement of the heat transfer to the olive stone particles when the fluidization is more vigorous [3,45]. Independently of the value of U/U_{mf}, a match of the estimation of the LCM-DAEM model to the experimental measurements can be found, proving the capability of the model to predict the evolution of the olive stones pyrolysis in a BFB reactor.

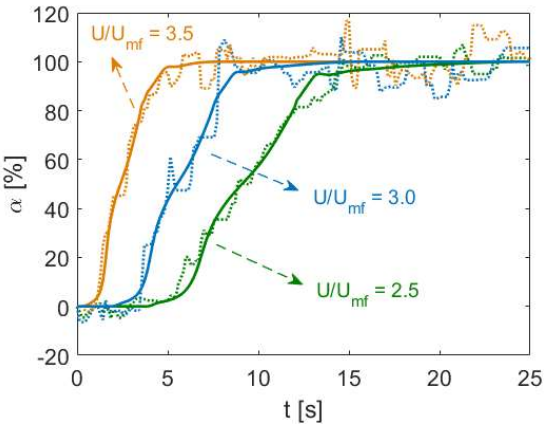

Figure 7: Comparison of the LCM-DAEM estimations (solid lines) and the experimental measurements (dotted lines) for the time evolution of the conversion degree during the pyrolysis of olive stones in a BFB reactor for various dimensionless gas velocities (T_∞ = 500 ºC, d_{os} = 1.15 – 1.60 mm).

The characteristic heating time τ obtained from the fitting of the estimations of the LCM-DAEM model, Eq. (5), to the experimental measurements is plotted in Figure 8 a), for each value of the dimensionless gas velocity. An almost linear reduction of the characteristic heating time of the olive stone particles in the BFB with the dimensionless gas velocity was found. This reduction can be attributed to the increase of the convection coefficient *h* inside the bed with the gas velocity, which is stronger for low values of the dimensionless gas velocity U/U_{mf} as those selected in this study [46, 47]. This result is in good agreement with the increase of the global convection coefficient with U/U_{mf} from a fluidized bed to a fuel particle predicted by the correlation proposed by Chao et al. [47], considering both gas-solid and solid-solid convection. Figure 8 b) shows the effect of U/U_{mf} on the pyrolysis time t_{pyr}, defined as the time for which the conversion degree estimated by the LCM-DAEM model attains α = 95 %. Since the bed temperature is T_∞ = 500 ºC for all the values of U/U_{mf} in this case, there is a direct relation between the characteristic heating time τ and the pyrolysis time t_{pyr}, obtaining a similar reduction of the pyrolysis time with the dimensionless gas velocity. The pyrolysis time of olive stones of d_{os} = 1.15 – 1.60 mm in a BFB at T_∞ = 500 ºC can be reduced by 65 % by increasing the dimensionless gas velocity from U/U_{mf} = 2.5 to U/U_{mf} = 3.5, as shown in Figure 8 b). Comparing the values of the pyrolysis time t_{pyr} and the characteristic heating time τ, a direct relation of approximately $t_{pyr}/\tau \sim 2.2$ was found.

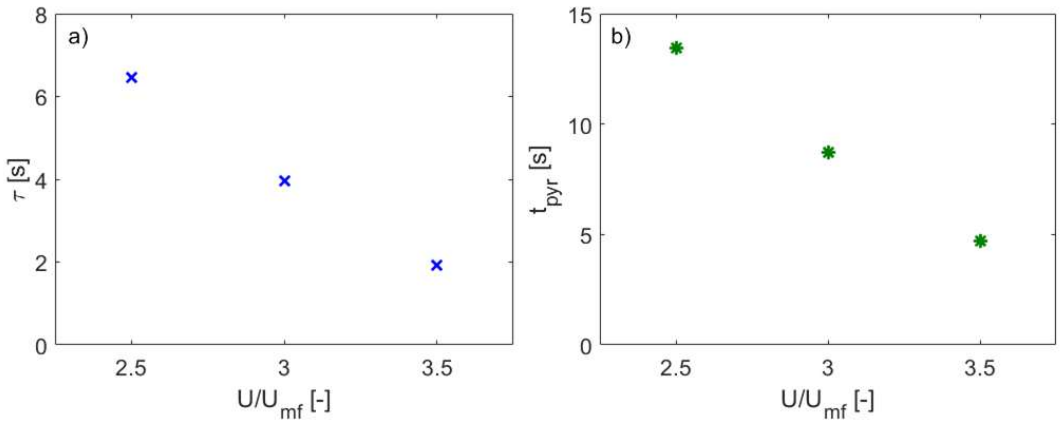

Figure 8: Effect of the dimensionless gas velocity on: a) characteristic heating time and b) pyrolysis time (T_∞ = 500 ºC, d_{os} = 1.15 – 1.60 mm).

4.4. Effect of bed temperature

The analysis of the reactor temperature effect was performed operating the bed at U/U_{mf} = 3.0 and pyrolyzing olive stones with particle sizes of d_{os} = 1.15 – 1.60 mm. The bed temperatures tested were 500, 550, and 600 ºC. Figure 9 shows the comparison of the experimental measurement of the time evolution of α and the prediction of the LCM-DAEM model, obtaining a proper agreement. The increase of bed temperature also accelerates the pyrolysis process [22,23], as a result of the higher availability of thermal energy in the reactor. Therefore, biomass particles release their volatile matter faster and, as a result, the feeding rate could be increased for higher temperatures. However, this result should be considered carefully if the liquid yield obtained from biomass pyrolysis is to be maximized for an optimal bio-oil production, since for temperatures above 600 ºC secondary cracking reactions may occur, reducing the amount of liquid yield in favor of permanent gas formation [2]. In fact, there is an optimal temperature for the maximization of the liquid yield produced from biomass pyrolysis that

varies between 450 and 550 ºC [42], depending mainly on the feedstock pyrolyzed [48].

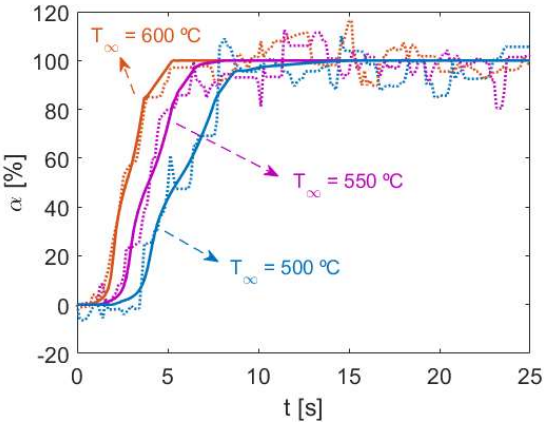

Figure 9: Comparison of the LCM-DAEM estimations (solid lines) and the experimental measurements (dotted lines) for the time evolution of the conversion degree during the pyrolysis of olive stones in a BFB reactor for various reactor temperatures (U/U_{mf} = 3.0, d_{os} = 1.15 – 1.60 mm).

The characteristic heating time of the olive stone particles obtained from the fitting of the model to the experimental data obtained for different reactor temperatures is plotted in Figure 10 a). Similar values for the characteristic heating time τ were obtained independently of the bed temperature. This is a plausible result considering the definition of τ, Eq. (2), which depends on characteristics of the biomass particles used, namely ρ_s, V_s, A_s, and c_s, and the convection coefficient h. For the tests varying the bed temperature, the characteristics of the olive stone particles are constant since neither the particle size nor the biomass used were changed. Furthermore, the convective coefficient depends mainly on the gas velocity, which is also the same for all the bed temperatures tested, obtaining only slight variations of h with temperature due to the effect of temperature on the fluidizing gas properties. In contrast to

the characteristic heating time, the pyrolysis time t_{pyr} is reduced when the bed temperature is increased, as shown in Figure 10 b), due to the faster pyrolysis process. Therefore, a direct relation between the characteristic heating time τ and the pyrolysis time t_{pyr} could not be found as a consequence of the different reactor temperatures in each case. The characteristic heating time is the time for which the ratio $(T_\infty - T)/(T_\infty - T_0)$ has been reduced by a factor of e. This means that, considering an initial temperature for the olive stone particles of T_0 = 20 ºC, the temperature of the biomass particles after the characteristic heating times shown in Figure 10 a), will be T = 323, 355, and 387 ºC for bed temperatures of T_∞ = 500, 550, and 600 ºC, respectively. Hence, the higher biomass temperature for higher bed temperature results in a greater pyrolysis conversion degree for the similar values of τ obtained for all the temperatures tested, causing a reduction of the pyrolysis time t_{pyr}, as shown in Figure 10 b).

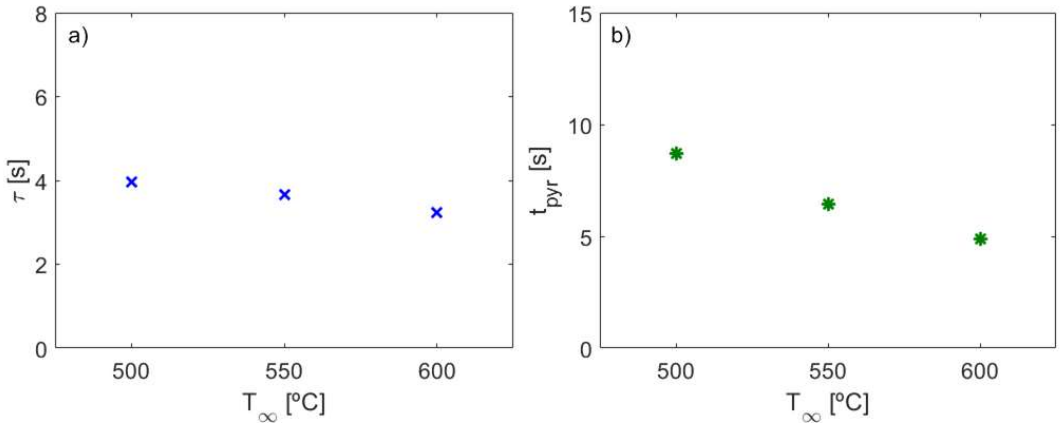

Figure 10: Effect of the bed temperature on: a) characteristic heating time and b) pyrolysis time (U/U_{mf} = 3.0, d_{os} = 1.15 – 1.60 mm).

In this case, the relation of the pyrolysis time t_{pyr} and the characteristic heating time τ depends on the bed temperature T_∞, obtaining t_{pyr}/τ = 2.2, 1.8, and 1.5

for T_∞ = 500, 550, and 600 ºC, respectively. These values correspond to an inverse relation of the ratio t_{pyr}/τ with the bed temperature T_∞ in the form

$$\frac{t_{pyr}}{\tau} = \frac{440}{T_\infty - 300}, \tag{7}$$

with T_∞ in ºC. According to Eq. (7), bed temperatures above 300 ºC are required to pyrolyze olive stones, which is in agreement with the results obtained in the thermogravimetric analyzer, shown in Figure 2. However, higher reactor temperatures, T_∞ > 450 ºC, as those typically used in the literature [42], should be used to obtain reasonable values for the pyrolysis time. In practical use, Eq. (7) can be employed to estimate the pyrolysis time t_{pyr} of thermally small olive stone particles from the calculation of the characteristic heating time τ, by Eq. (2), for the bed temperature employed. This pyrolysis time can be used to determine an optimal biomass feeding rate, considering the ratio biomass to inert material desired in the BFB for a stable operation.

4.5. Effect of particle diameter

The effect of the olive stone particle size on the pyrolysis process was also tested. In this case, both the bed temperature and the dimensionless gas velocity were maintained constant at values of T_∞ = 550 ºC and U/U_{mf} = 3.0. The crushed olive stones were sieved to obtain four different ranges of particle sizes of d_{os} = 1.25 – 1.60, 1.60 – 2.00, 2.00 – 2.50, and 2.50 – 3.15 mm. The time evolution of the pyrolysis conversion degree measured for the various olive stone particle sizes tested are depicted in Figure 11. No results of the LCM-DAEM model estimations are represented in this case to improve visualization of the figure, since no significant differences are obtained for the biomass

particle sizes tested. This independence of the pyrolysis conversion degree on the particle size is a proof of the thermally small character of the biomass particles used.

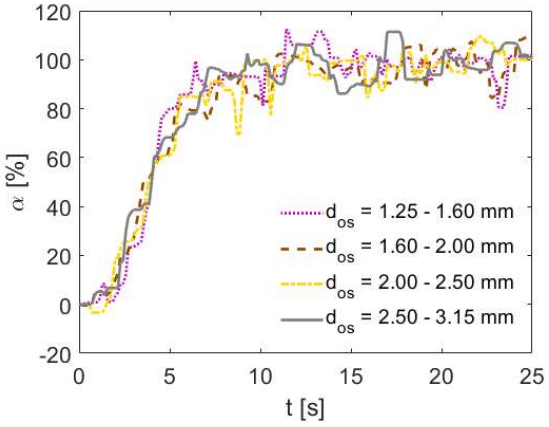

Figure 11: Experimental measurements for the time evolution of the conversion degree during the pyrolysis of olive stones in a BFB reactor for various biomass particle sizes (T_∞ = 550 ºC, U/U_{mf} = 3.0).

Although the estimations of the LCM-DAEM model for the time evolution of α are not included in Figure 11, the results of the optimal characteristic heating time τ and pyrolysis time t_{pyr} for each particle size are plotted in Figure 12. In this case, the characteristic heating time of the different biomass particles is very similar and, since the tests for different particle sizes were all conducted for the same bed temperature, T_∞ = 550 ºC, a direct relation between the characteristic heating time and the pyrolysis time is obtained. Therefore, the pyrolysis time is independent of the olive stone particle size for the range of particle sizes tested, 1.25 mm < d_{os} < 3.15 mm, confirming the hypothesis of thermally small particles. Provided that the particles are thermally small, the temperature inside the particle will be uniform and they will be heated at the same rate, controlled by the thermal convection resistance at their surface,

obtaining the same heating profile for all the particle sizes and, thus, resulting in a pyrolysis time independent of the particle size considered. As shown in Figure 12, the ratio t_{pyr}/τ is independent of the olive stone average particle sizes employed, being approximately $t_{pyr}/\tau \sim 1.8$ for $d_{os} < 3.15$ mm.

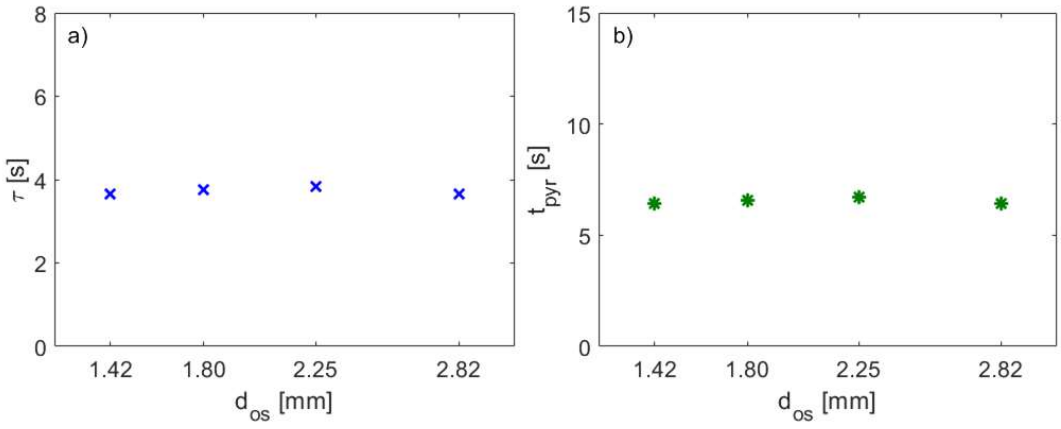

Figure 12: Effect of the average olive stone particle size on: a) characteristic heating time and b) pyrolysis time (T_∞ = 550 ºC, U/U_{mf} = 3.0).

The low pyrolysis times obtained in this work are in good agreement with the literature, considering the low particle size of the crushed olive stones employed to ensure the fulfilment of the condition of thermally small particles. In fact, the correlation proposed by Leckner [49] for the devolatilization time of solid fuel particles predicts reaction times below 10 s for particle diameters under 3.15 mm, as those selected in this study. Furthermore, Wang et al. [50] measured similar pyrolysis times for beech wood particles with diameters below 3 mm in a fluidized bed, proving also the thermally small character of these fine particles. However, their measured pyrolysis times increased fast for larger particles. This effect of particle size on the pyrolysis time and the constant value obtained for low particle diameters are also predicted by the correlations of Chan et al. [51],

Thurner and Mann [52], and Di Blasi and Branca [53], from which similar values are derived for the pyrolysis time compared to those measured in this work.

5. Conclusions

The pyrolysis of crushed olive stones was studied experimentally in a lab scale BFB reactor installed on a scale. The pyrolysis measurements were conducted varying the fluidized bed temperature, the inert fluidizing gas velocity, and the olive stone particle sizes. The activation energy and pre-exponential factor of the olive stone pyrolysis were determined applying the simplified DAEM to pyrolysis measurements conducted in a thermogravimetric analyzer. These kinetic parameters were employed as an input of a model combining transient heat transfer to the biomass particles, described by the LCM, and chemical kinetics of the pyrolysis reaction, accounted for by the simplified DAEM. The combined LCM-DAEM model was validated with the experimental measurements, obtaining a proper agreement for the time evolution of the conversion degree estimated by the model and derived from the experimental measurements. Low pyrolysis times, under 15 s, were obtained in all cases due to the small particle size of the crushed olive stones. In fact, the similar values of the pyrolysis time attained for all the particle sizes analyzed, below 3.15 mm, guarantee the thermally small character of the biomass particles used. Furthermore, an inverse relation for the ratio of pyrolysis time to characteristic heating time with the bed temperature was found.

Acknowledgments

The authors express their gratitude to the BIOLAB experimental facility and to the program “Research Stays for University Academics and Scientists” from the

German Academic Exchange Service (DAAD) for the financial support conceded to Antonio Soria-Verdugo for a research stay at the German Aerospace Center DLR (Stuttgart, Germany) during the summer of 2019. Funding by Deutsches Zentrum für Luft- und Raumfahrt e. V. (DLR), the German Aerospace Center, and the Helmholtz Association in the research fields energy, fuels and gasification, especially in the Program “Energy Efficiency, Materials and Resources“ Topic 4 “Efficient Use of Fuel Resources“ is also gratefully acknowledged.

References

[1] Bridgwater A.V. Review of fast pyrolysis of biomass and product upgrading. Biomass Bioenerg. 2012; 38, 68-94.

[2] Pütün A.E., Apaydin E., Pütün E. Bio-oil production from pyrolysis and steam pyrolysis of soybean-cake: product yields and composition. Energy 2002; 27, 703-713.

[3] Bridgwater A.V., Meier D., Radlein D. An overview of fast pyrolysis of biomass. Org. Geochem. 1999; 30, 1479-1493.

[4] Bridgwater A.V., Peacocke G.V.C. Fast pyrolysis processes for biomass. Renew. Sust. Energ. Rev. 2000; 4, 1-73.

[5] Gao Z., Li N., Yin S., Yi W. Pyrolysis behavior of cellulose in a fixed bed reactor: Residue evolution and effects of parameters on products distribution and bio-oil composition. Energy 2019; 175, 1067-1074.

[6] Pielsticker S., Schlögel K., Kreitzberg T., Hatzfeld O., Kneer R. Biomass pyrolysis kinetics in a fluidized bed reactor: Measurements and plausibility verification for reaction conditions. Fuel 2019; 254, 115589.

[7] Olazar M., Lopez G., Amutio M., Elordi G., Aguado R., Bilbao J. Influence of FCC catalyst steaming on HDPE pyrolysis product distribution. J. Anal. Appl. Pyrolysis 2009; 85, 359-365.

[8] Wagenaar B.M., Prins W., Swaaij W.P.M. Pyrolysis of biomass in the rotating cone reactor: modelling and experimental justification. Chem. Eng. Sci. 1994; 49, 5109-5126.

[9] Wise H.G., Dichiara A.B., Resende F.L.P. Ex-situ catalytic fast pyrolysis of Beetle-killed lodgepole pine in a novel ablative reactor. Fuel 2019; 241, 933-940.

[10] Silvestre W.P., Pauletti G.F., Godinho M., Baldasso C. Fodder radish seed cake pyrolysis for bio-oil production in a rotary kiln reactor Chem. Eng. Process. 2018; 124, 235-244.

[11] Tomasi Morgano M., Leibold H., Richter F., Stapf D., Seifert H. Screw pyrolysis technology for sewage sludge treatment. Waste Manage. 2018; 73, 487-495.

[12] Ellens C.J., Brown R.C. Optimization of a free-fall reactor for the production of fast pyrolysis bio-oil. Bioresource Technol. 2012; 103, 374-380.

[13] Martín M.T., Sanz A.B., Nozal L., Castro F., Alonso R., Aguirre J.L., González S.D., Matía M.P. Novella J.L., Peinado M. Vaquero J.J. Microwave-

assisted pyrolysis of Mediterranean forest biomass waste: Bioproduct characterization. J. Anal. Appl. Pyrolysis 2017; 127, 278-285.

[14] Roy C. Chaala A., Darmstadt H. The vacuum pyrolysis of used tires: end uses for oil and carbon black products. J. Anal. Appl. Pyrolysis 1999; 51, 201-221.

[15] Lin Y.C., Wu T.Y., Jhang S.R., Yang P.M., Hsiao Y.H. Hydrogen production from banyan leaves using an atmospheric-pressure microwave plasma reactor. Bioresource Technol. 2014; 161, 304-309.

[16] Fan H., He K. Fast pyrolysis of sewage sludge in a Curie-point pyrolyzer: The case of sludge in the city of Shanghai, China. Energ. Fuel. 2016; 30, 1020-1026.

[17] Coats A.W., Redfern J.P. Kinetic parameters from thermogravimetric data. Nature 1964; 201, 68-69.

[18] Li Z., Zhao W., Meng B., Liu C., Zhu Q., Zhao G. Kinetic study of corn straw pyrolysis: comparison of two different three-pseudo component models. Bioresource Technol. 2008; 99, 7616-7622.

[19] Vyazovkin S. Isoconversional kinetics. In: Handbook of Thermal Analysis and Calorimetry 2008; Vol. 5 : Recent Advances, Techniques and Applications, Brown M.E. and Gallagher P.K (Editors), Elsevier B. V., 503-538.

[20] Vand V. A theory of the irreversible electrical resistance changes of metallic films evaporated in vacuum. Proc. Phys. Soc. 1943; 55, 222-246.

[21] Soria-Verdugo A., Rubio-Rubio M., Goos E., Riedel U. Combining the lumped capacitance method and the simplified distributed activation energy model to describe the pyrolysis of thermally small biomass particles. Energ. Convers. Manage. 2018a; 175, 164-172.

[22] Soria-Verdugo A., Morato-Godino A., Garcia-Gutierrez L.M., García-Hernando N. Pyrolysis of sewage sludge in a fixed and a bubbling fluidized bed – Estimation and experimental validation of the pyrolysis time. Energ. Convers. Manage. 2017a; 144, 235-242.

[23] Morato-Godino A., Sánchez-Delgado S., García-Hernando N., Soria-Verdugo A. Pyrolysis of *Cynara cardunculus* L. samples – Effect of operating conditions and bed stage on the evolution of the conversion. Chem. Eng. J. 2018; 351, 371-381.

[24] Incropera F.P., De Witt D.P., Bergman T.L., Lavine A.S. Fundamentals of heat and mass transfer, 6th ed., John Wiley & Sons, United States of America, 2007.

[25] Miura K. A new and simple method to estimate f(E) and k_0(E) in the distributed activation energy model from three sets of experimental data. Energ. Fuel. 1995; 9, 302-307.

[26] Miura K., Maki T. A simple method for estimating f(E) and k_0(E) in the distributed activation energy model. Energ. Fuel. 1998; 12, 864-869.

[27] Günes M., Günes S.K. Distributed activation energy model parameters of some Turkish coals. Energ. Source. Part A 2008; 30, 1460-1472.

[28] Li Z., Liu C., Chen Z., Qian J., Zhao W., Zhu Q. Analysis of coals and biomass pyrolysis using the distributed activation energy model. Bioresource Technol. 2009; 100, 948-952.

[29] Várghegyi G., Szabó P., Antal M.J. Kinetics of charcoal devolatilization. Energ. Fuel. 2002; 16, 724-731.

[30] Soria-Verdugo A., García-Hernando N., Garcia-Gutierrez L.M., Ruiz-Rivas U. Analysis of biomass and sewage sludge devolatilization using the distributed activation energy model. Energ. Convers. Manage. 2013; 65, 239-244.

[31] Wanjun T., Cunxin W., Donghua C. Kinetic studies on the pyrolysis of chitin and Chitosan. Polym. Degrad. Stab. 2005; 87, 389-394.

[32] Cai J., Liu R. New distributed activation energy model: numerical solution and application to pyrolysis kinetics of some types of biomass. Bioresource Technol. 2008; 99, 2795-2799.

[33] Soria-Verdugo A., Garcia-Gutierrez L.M., Blanco-Cano L., Garcia-Hernando N., Ruiz-Rivas U. Evaluating the accuracy of the Distributed Activation Energy Model for biomass devolatilization curves obtained at high heating rates. Energ. Convers. Manage. 2014; 86, 1045-1049.

[34] Yan J.H., Zhu H.M., Jiang X.G., Chi Y., Cen K.F. Analysis of volatile species kinetics during typical medical waste materials pyrolysis using a distributed activation energy model. J. Hazard. Mater. 2009; 162, 646-651.

[35] Soria-Verdugo A., Goos E., Morato-Godino A., García-Hernando N., Riedel U. Pyrolysis of biofuels of the future: Sewage sludge and microalgae -

Thermogravimetric analysis and modelling of the pyrolysis under different temperature conditions. Energ. Convers. Manage. 2017b; 138, 261-272.

[36] Soria-Verdugo A., Goos E., García-Hernando N., Riedel U. Analyzing the pyrolysis kinetics of several microalgae species by various differential and integral isoconversional kinetic methods and the Distributed Activation Energy Model. Algal Res. 2018b; 32, 11-29.

[37] Soria-Verdugo A., Goos E., Arrieta-Sanagustín J., García-Hernando N. Modeling of the pyrolysis of biomass under parabolic and exponential temperature increases using the Distributed Activation Energy Model. Energ. Convers. Manage. 2016; 118, 223-230.

[38] Christoforou E., Fokaides P.A., A review of olive mill solid wastes to energy utilization techniques. Waste Management 2016; 49, 346-363.

[39] De Palma K.R., García-Hernando N., Silva M.A., Tomaz E., Soria-Verdugo A. Pyrolysis and combustion kinetic study and complementary study of ash fusibility behavior of sugarcane bagasse, sugarcane straw, and their pellets - Case study of agro-industrial residues. Energ. Fuel. 2019; 33(4), 3227-3238.

[40] Soria-Verdugo A., Goos E., García-Hernando N. Effect of the number of TGA curves employed on the biomass pyrolysis kinetics results obtained using the Distributed Activation Energy Model. Fuel Process. Technol. 2015; 134, 360-371.

[41] Koppatz S., Pfeifer C., Hofbauer H. Comparison of the performance behavior of silica sand and olivine in a dual fluidized bed reactor system for

steam gasification of biomass as a pilot plant scale. Chem. Eng. J. 2011; 175, 468-483.

[42] Guedes R.E., Luna A.S., Torres A.R. Operating parameters for bio-oil production in biomass pyrolysis: A review. J. Anal. Appl. Pyrolysis 2018; 129, 134-149.

[43] Li Z., Zhao W., Meng B., Liu C., Zhu Q., Zhao G. Kinetic study of corn straw pyrolysis: Comparison of two different three-pseudocomponent models. Bioresource Technol. 2008; 99, 7616-7622.

[44] Anca-Couce A. Reaction mechanisms and multi-scale modelling of lignocellulosic biomass pyrolysis. Prog. Energ. Combust. 2016; 53, 41-79.

[45] Yan Q., Toghiani H., Yu F., Cai Z., Zhang J. Effects of pyrolysis conditions on yield of bio-chars from pine chips. Forest Prod. J. 2011; 61, 367-371.

[46] Davidson J.F., Harrison D. Fluidization. Academic Press, London and New York, 1971.

[47] Chao J., Lu J., Yang H., Zhang M., Liu Q. Experimental study on the heat transfer coefficient between a freely moving sphere and a fluidized bed of small particles. Int. J. Heat Mass Tran. 2015; 80, 115-125.

[48] Biswas B., Pandey N., Bisht Y., Singh R., Kumar J., Bhaskar T. Pyrolysis of agricultural biomass residues: comparative study of corn cob, wheat straw, rice straw and rice husk. Bioresource Technol. 2017; 237, 57-63.

[49] Leckner B. Fluidized bed combustion: achievements and problems. Proc. Combust. Inst. 1996; 26, 3231-3241 1996; 3231-3241.

[50] Wang X., Kersten S.R.A., Prins W., van Swaaij W.P.M. Biomass Pyrolysis in a Fluidized Bed Reactor. Part 2: Experimental Validation of Model Results. Ind. Eng. Chem. Res. 2005; 44, 8786-8795.

[51] Chan W.C.R., Kelbon M., Krieger B.B. Modelling and experimental verification of physical and chemical processes during pyrolysis of a large biomass particle. Fuel 1985, 64; 1505-1513.

[52] Thurner F., Mann U. Kinetic investigation of wood pyrolysis. Ind. Eng. Chem. Process Des. Dev. 1981; 20, 482-488.

[53] Di Blasi C., Branca C. Kinetics of primary product formation from wood pyrolysis. Ind. Eng. Chem. Res. 2001; 40, 5547- 5556.

List of figures

Figure 9: Comparison of the LCM-DAEM estimations (solid lines) and the experimental measurements (dotted lines) for the time evolution of the conversion degree during the pyrolysis of olive stones in a BFB reactor for various reactor temperatures (U/U_{mf} = 3.0, d_{os} = 1.15 – 1.60 mm).

Figure 10: Effect of the bed temperature on: a) characteristic heating time and b) pyrolysis time (U/U_{mf} = 3.0, d_{os} = 1.15 – 1.60 mm).

Figure 11: Experimental measurements for the time evolution of the conversion degree during the pyrolysis of olive stones in a BFB reactor for various biomass particle sizes (T_∞ = 550 ºC, U/U_{mf} = 3.0).

Figure 12: Effect of the average olive stone particle size on: a) characteristic heating time and b) pyrolysis time (T_∞ = 550 ºC, U/U_{mf} = 3.0).

List of tables